

# Jitter Test Program and On-Orbit Mitigation Strategies for Solar Dynamic Observatory

Kuo-Chia Liu, Thomas Kenney, Peiman Maghami, Pete Mule  
*NASA Goddard Space Flight Center, Greenbelt, MD, 20771*

Carl Blaurock  
*Nightsky Systems, Inc., 3916 Lauriston Rd, Raleigh NC 27616*

William B Haile  
*ATK Space Systems, Inc., 5050 Powder Mill Road, Beltsville, MD 20705 USA*

**The Solar Dynamic Observatory (SDO) aims to study the Sun's influence on the Earth, the source, storage, and release of the solar energy, and the interior structure of the Sun. During science observations, the jitter stability at the instrument focal plane must be maintained to less than a fraction of an arcsecond for two of the SDO instruments. To meet these stringent requirements, a significant amount of analysis and test effort has been devoted to predicting the jitter induced from various disturbance sources. This paper presents an overview of the SDO jitter analysis approach and test effort performed to date. It emphasizes the disturbance modeling, verification, calibration, and validation of the high gain antenna stepping mechanism and the reaction wheels, which are the two largest jitter contributors. This paper also describes on-orbit mitigation strategies to protect the system from analysis model uncertainties. Lessons learned from the SDO jitter analyses and test programs are included in the paper to share the knowledge gained with the community.**

## I. Introduction

The Solar Dynamic Observatory (SDO) is scheduled for launch in January 2009. The main science objective of this mission is to observe the Sun and increase the understanding of the Sun's influence on the Earth. There are three instruments onboard the SDO for achieving its scientific goals: the Atmospheric Imaging Assembly (AIA), the Helioseismic and Magnetic Imager (HMI), and the Extreme Ultraviolet Variability Experiment (EVE). Both AIA and HMI are sensitive to high frequency pointing perturbations and have sub-arcsecond level line-of-sight (LOS) jitter requirements. Extensive modeling and analysis efforts have been directed in estimating the amount of jitter disturbing the science instruments. In order to verify the disturbance models and to validate the jitter performance prior to launch, many jitter-critical components and subassemblies were tested either by the mechanism vendors or at the NASA Goddard Space Flight Center (GSFC).

A schematic of the SDO jitter test plan and the disturbance-to-performance flow is shown in Figure 1. The test plan consisted of hardware component tests, structural component tests, and assembly level tests. The hardware component test results were used for calibrating the disturbance input models which drove the observatory structural and optical models used to predict the LOS jitter performance. The structural component tests provided data for updating the structural finite element model (FEM). The test plan also included two assembly level tests, high gain antenna (HGA) and structural verification unit (SVU), for validating the jitter analysis process and the structural FEM. The HGA assembly tests included two HGA proto-flight gimbals, the flight HGA dish, and other flight-like supporting structures. The SVU is a duplicate of the flight structure and was used in conjunction with a flight reaction wheel to test the disturbance levels generated by the wheel. Additional spacecraft damping information was extracted from SVU stinger tests which demonstrated that the damping ratio used in the jitter analysis was reasonable.

This paper provides an overview of the SDO jitter test program and jitter analysis approach. The paper emphasizes the checks conducted for each of the analysis models and how test data were used to enhance the fidelity of the models. Brief descriptions of the test setup and relevant results are also included in the paper. Since the flight vehicle will not have "end-to-end" disturbance to LOS tests on the ground, there will still be several sources of uncertainties in the analysis. To protect against those uncertainties, on-orbit mitigation plans were created with jitter

test algorithms implemented in simulation. After discussing the on-orbit plans, the paper concludes with some lessons learned from the SDO jitter analysis and test program.

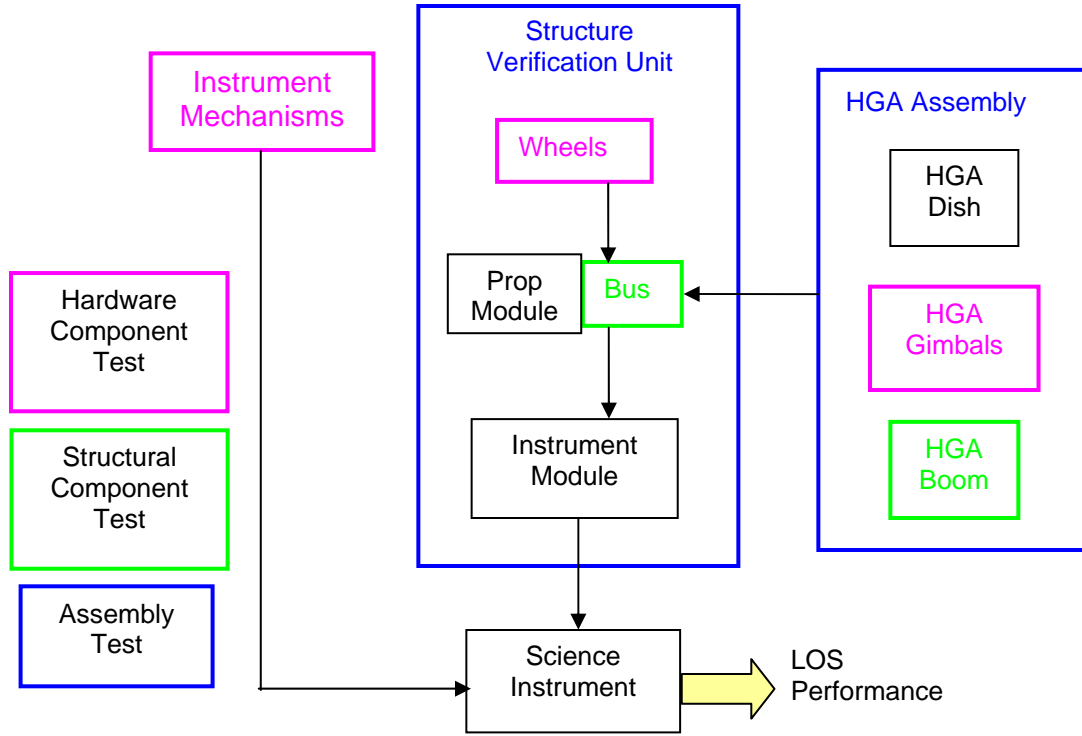


Figure 1 SDO Jitter Test Plan and Disturbance-to-Performance Flow

## II. Analysis Overview

The SDO jitter performance is defined as the line-of-sight (LOS) motion measured at the instrument detectors. The spacecraft attitude control system (ACS) is capable of removing large, slowly varying LOS (or pointing) errors. Both AIA and HMI have additional instrument stabilization systems (ISS) to reduce mid-frequency range LOS disturbances. The residual LOS motion, after ACS and ISS compensation, measured on the instrument detectors must be less than  $0.17$  arcsecond  $1-\sigma$  for AIA and  $0.14$  arcsecond  $1-\sigma$  for HMI.

### A. Jitter Analysis Approaches

There are two jitter evaluation metrics used in estimating SDO jitter performance. The first metric is a frequency-domain based evaluation method defined by the SDO scientists:

$$\sigma_j = \left[ \int_{-\infty}^{\infty} S_{zz}(\omega) |G_{ATF}(\omega)|^2 (1 - \text{sinc}^2(\omega\tau)) d\omega \right]^{1/2} \quad (1)$$

where  $\sigma_j$  is the root-mean-square (RMS) or  $1-\sigma$  jitter,  $S_{zz}$  is the power spectral density (PSD) of the LOS motion,  $G_{ATF}$  is the attenuation transfer function (ATF) that models the ISS performance,  $\omega$  is frequency in Hz, and sinc is a function defined as  $\text{sinc}(x) = \sin(x)/x$ . The variable  $\tau$  is the instrument exposure or integration time. The AIA telescopes have large exposure time variations that range from 0.1 sec to 3.0 sec, whereas the HMI exposure time has a smaller time range of 0.15-0.3 sec. The frequency-domain based jitter metric is appropriate for analyzing random disturbance inputs. However, many of the jitter sources are not random and their jitter effects can be analyzed using time-domain simulations. A second jitter performance metric used for non-random types of jitter effects is defined as follows<sup>1</sup>:

$$\sigma_j^2(\tau) = E \left\langle (\theta(t) - \bar{\theta}_\tau)^2 \right\rangle_\tau = \frac{1}{N-1} \sum_{n=M_1}^{M_2} (\theta[n] - \bar{\theta}_\tau)^2 \quad (2)$$

$$\bar{\theta}_\tau = \langle \theta(t) \rangle_\tau = \frac{1}{N} \sum_{n=M_1}^{M_2} \theta[n],$$

$$N = M_2 - M_1 + 1 = \frac{\tau}{\Delta t}$$

where  $\theta(t)$  is the LOS motion,  $N$  is the number of sampled data points in a sliding window with width  $\tau$ ,  $M_1$  is the initial index of the sliding window,  $M_2$  is the end index of the window, and  $dt$  is the simulation sample time. The jitter prediction is calculated using either Eq. (1) for frequency-domain analysis or Eq. (2) for time-domain simulations. The jitter predictions and various sensitivity analyses were performed using Matlab, Simulink, and Nightsky Systems Inc.'s Disturbance-Optics-Controls-Structures (DOCS) Toolbox.

## B. Integrated Modeling and Model Check Approaches

The SDO jitter analysis employs an integrated modeling approach where disturbance, structures, controls, and performance metrics are combined into one dynamic model to predict the end-to-end LOS performance of the system. Figure 2 is a functional diagram of all the sub-system models used in the integrated model. The disturbance models are inputs to the system, the structural model is created from the finite element analysis, the ACS model stabilizes the rigid body modes of the structural model, the optical model maps all the optical motions to the LOS motion, and the instrument stabilization system (ISS) models the LOS motion attenuation from the instrument controllers. The outputs from the integrated model are the LOS motion measured at the AIA and HMI charged coupled devices (CCDs).

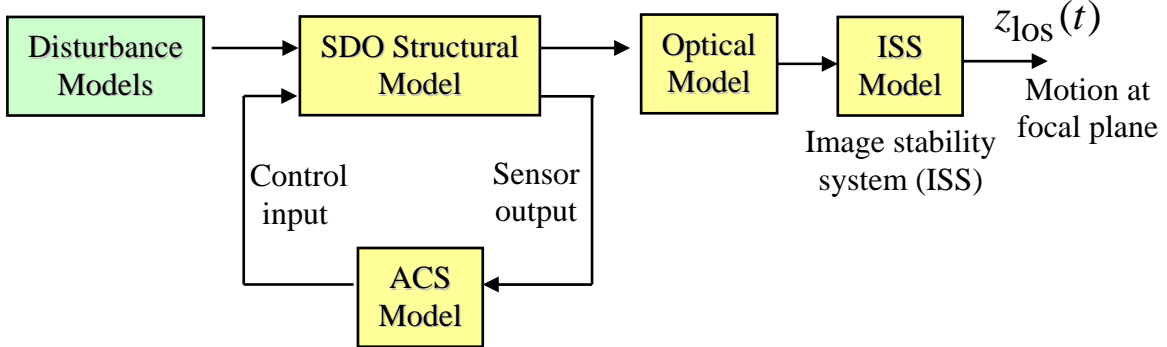


Figure 2 SDO integrated model

The yellow boxes in Figure 2 represent common elements to all disturbance analyses. These common analysis models will be described in more detail in Section III. There are several disturbance sources onboard the observatory. The two largest jitter contributors are the HGA stepper motors and the reaction wheels. Other sources include the instrument mechanisms, and the ACS actuators (e.g. wheel torque quantization) and sensor noises that also introduce jitter through the ACS closed-loop system. This paper focuses on the tests performed to verify, calibrate, and validate the HGA model in Section IV and wheel disturbance model in Section V.

Before discussing the SDO jitter team's model check approaches, the following definitions will help the discussions in the rest of the paper:

- Verification: The process of determining that a computational model accurately represents the underlying mathematical model and its solution<sup>2</sup>.
- Validation: The process of determining the degree to which a model is an accurate representation of the real world from the perspective of the intended uses of the model<sup>3</sup>.
- Calibration: The process of adjusting numerical or physical modeling parameters in the computational model for the purpose of improving agreement with experimental data<sup>3</sup>.



Model verification was performed through model verification checks. The FEM was subject to a Unit Enforced Displacement and Rotation check, to verify that no illegal grounding was present in the model, and Free-Free Dynamics with a Stiffness Equilibrium check to verify that the model acts as a rigid body when it is unconstrained. The Stiffness Equilibrium check also checks the stiffness matrix to verify that there were no grounding effects.

Model calibration and validation involved correlating the model to modal and frequency response test data. The model was reduced to represent the test configurations and changes to the reduced model were incorporated into observatory jitter FEM. Primary structure FEM was calibrated through a modal survey that targeted the primary high mass modes of the observatory out to 60 Hz. Secondary structure and instrument models were calibrated through matching frequency response from tap and vibration testing. Differences in test and analytical predictions were found primarily to be a result of insufficient fidelity in specific areas of the model. Off-line high fidelity models were created for the complex HGAS bracketry to improve model correlation. Stiffness values from the off-line models were incorporated into the observatory model.

The normal modes solution of MSC/NASTRAN was run on the unconstrained FEM, and mode shape and frequency data for a subset of 120 nodes was provided to the jitter group. The model was run in five different HGAS gimballed orientations to assess their effects on jitter. The Residual Vector augmentation method was used to generate auxiliary modes containing the additional contributions needed to match the static shape of gimballed rotations. This was done by applying equal and opposite moment loads to each actuator separately using NASTRAN LSEQ cards in the normal modes analysis run. The analysis runs produced over 650 modes between 0 and 200 Hz.

## B. Damping Model

The damping model assumed uncoupled modal damping. The scalar damping value, used for all modes, was calibrated by test. The test article comprised the Structural Verification Unit bus, the flight Instrument Module, 3 AIA mass simulators and one AIA dynamic simulator, and an HMI mass simulator (Figure 5). The bus was mounted on air bags to give flight-like boundary conditions. The test article was excited using a proof mass actuator through a force-gage-equipped stinger. Tests at several forcing levels (at least two, three if noise level permitted) provided amplitude dependence information. Frequency Response Functions (FRFs) from input force to 19 accelerometer responses were acquired with a DataMax data acquisition system. The FRFs were fit with system identification tools to produce a total of 88 Single Input, Multiple Output (SIMO) state space models representing different amplitudes, input locations, and accelerometer outputs. A total of 1234 modes in the 20-200 Hz range were extracted. The average response levels of 7 to 46 milli-g's, depending on forcing amplitude, were linearly extrapolated to the flight level of about 0.5 milli-g's. The resulting damping set was binned into 0.1% damping histograms (Figure 6). The resulting damping histogram shows a peak at 0.4% damping, with about 5% of the modes below 0.3% damping. The baseline damping value was set at 0.3%.



Figure 5 SVU jitter test configuration

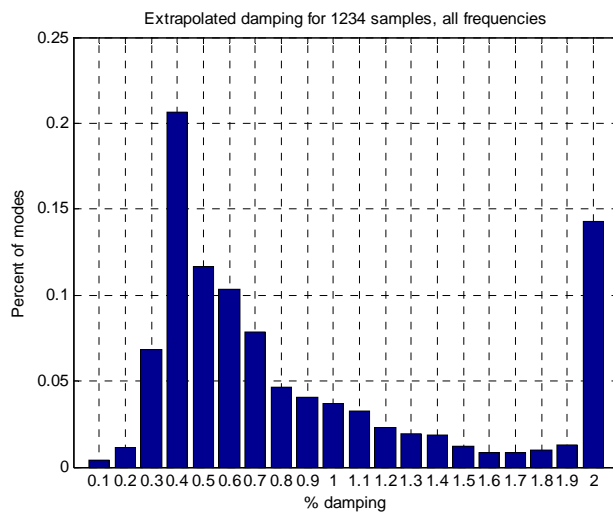


Figure 6 SDO jitter test damping histogram

### C. Optical model

The optical ray trace models for AIA and HMI were provided by analysts at the Lockheed Martin Solar and Astrophysics Lab (LMSAL). Using the optical models, the analyst perturbed each DOF of all the optical elements and recorded the resulting image shift on the CCD. At the end of this process, a linear matrix was created that maps the small optical motions to image motions measured on the CCD (e.g. LOS errors). This matrix is often referred to as the optical sensitivity matrix.

The optical ray trace model passed the unit rotation check verification test. The entire instrument was rotated rigidly about some angle, and the predicted motion on the CCD was equal to the specified angle rotation. A SDO jitter analyst also reconstructed the LMSAL ray trace model based on the optical descriptions and produced the same optical sensitivity matrix as the analyst at LMSAL.

The optical models were calibrated by LMSAL by measuring the focal length of the primary mirror, the secondary mirror, and the effective focal length of the telescope system. To validate the optical performance of the telescope, interferometry tests were performed at the Smithsonian Astrophysical Laboratory.

### D. Control models

SDO features two control systems that influence the pointing of the spacecraft: (1) attitude control system (ACS) and (2) instrument stabilization system (ISS). The ACS uses reaction wheels to stabilize rigid body pointing of the observatory. The ACS control system design, the wheel torque models, and the sensor models are provided by the ACS analysis team<sup>4</sup>. The attitude controller consists of a standard proportional-integral-derivative (PID) controller and a second-order structural filter for suppressing low frequency flexible modes and gain stabilizing the system. For jitter analysis, the main purpose of the ACS is to stabilize the three rigid-body modes. The ACS has no impact on the high frequency behavior or jitter motion of the closed-loop system. The ACS performance is verified by a high fidelity simulation developed by the SDO ACS team. Several ACS sensors and actuators have been tested to calibrate various models in the ACS simulation. System level performance tests with ACS hardware in the loop will also be conducted to validate the controller performance.

Both AIA and HMI have an ISS that further attenuates residual pointing errors around body Y and Z axes (or tip/tilt of the LOS vector) from the ACS. The ISS has much higher bandwidth than the ACS and does impact the jitter performance of the system. These controllers are designed and constructed by engineers at the LMSAL. Each AIA science telescope is accompanied by a guide telescope (GT) that uses limb sensors to provide pointing jitter signals to the ISS for image motion correction. The AIA ISS employs a PZT actuated tip/tilt secondary mirror located inside the science telescope to center the image on the CCD. Since the actuated mirror is not in the detection (optical) path of the limb sensor, the AIA has an open-loop ISS design. The performance of the AIA ISS will depend on the calibration of the GT error signal and the image motion introduced by the PZT actuator. HMI also has limb sensors to feed back error signals to its ISS which drives a tip/tilt mirror to reduce image motion. Unlike the AIA design, the actuated mirror for HMI is in the optical path of the limb sensor. Therefore, the HMI ISS system operates in a closed-loop mode.

The disturbance rejection capabilities of each ISS were modeled as high-pass filters. These models were verified by demonstrating that the magnitudes of the high-pass filters match the requirements on the ISS exactly. The actual performance of each of the ISS was tested by engineers at LMSAL. The test data were delivered to GSFC for calibrating and validating the ISS models. The left and right plots of Figure 7 illustrate the comparison between the ISS test data and the ISS model for AIA and HMI, respectively. As a note, when the test data showed better suppression than is required, the ISS model matches the required performance in order to add some conservatism to the analysis.

### E. Uncertainty

There are three types of uncertainties considered in the SDO jitter analysis. The first type is the modal gain uncertainty since the magnitudes of most of the high frequency modes are not validated by test data. To protect against the modal gain uncertainty, the jitter analysis team requires a 100% margin on the current best estimate (CBE) jitter when compared to the allocated requirements. The percent margin is defined as

$$\% \text{ margin} = \left( \frac{\text{Requirement}}{\text{CBE}} - 1 \right) * 100 \quad (3)$$

The second type of uncertainty is modal frequency. Only the frequencies of primary modes are matched to the test data, and the frequencies of other modes may easily vary 5-10% and possibly more. In order to estimate the impact

of modal frequency uncertainty on the analysis results, the jitter team performed frequency sensitivity analyses by either varying the FEM modes or the input disturbance frequencies by +/- 10% . The worst-case result from the frequency sweep studies was reported as CBE to guard against frequency uncertainty. The third type of uncertainty is on disturbance amplitude. With the exception of the HGA and wheels, most of the disturbance mechanisms only have partial test data available (i.e. not all three forces and three torques are measured). In those cases, the analysis team applied an additional factor (1.5-2.0) to the CBEs.

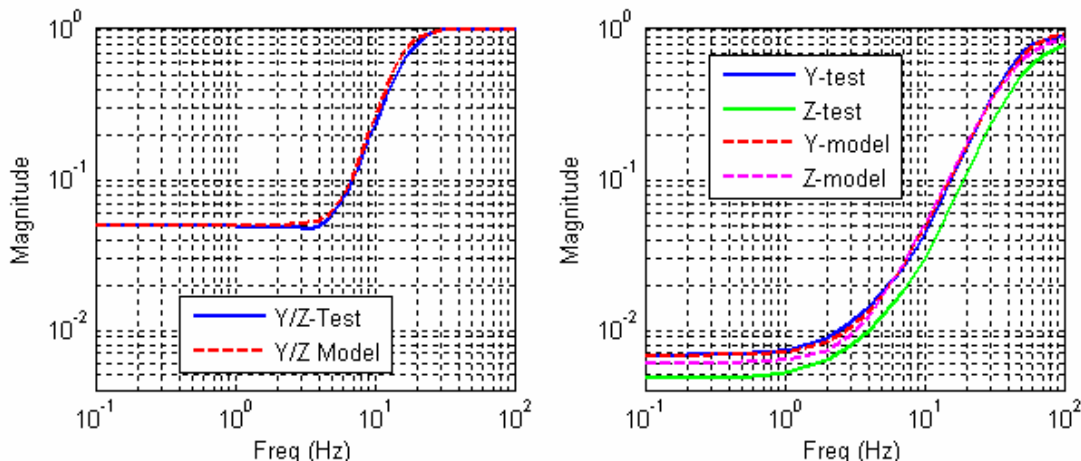


Figure 7 Instrument attenuation transfer function: (left) AIA ISS (right) HMI ISS

#### IV. HGA Disturbance Model

The High Gain Antenna System (HGAS) uses stepper motor actuators to drive each of the two antennae in two axes (Azimuth and Elevation). Each actuator consists of a 3-phase, 40-pole stepper motor (240 detents) actuating through a 200:1 harmonic drive, for a final output step size of 0.0075 degrees. Each actuator step imparts a small disturbance torque into the spacecraft. The sequence of steps as the actuators move to follow the commanded profile can interact in complex ways with the ring down from previous steps and from other actuators. Worst-case estimates of HGA-induced jitter showed that the allocations were violated by several hundred percent. A comprehensive analysis was therefore undertaken to determine the percentage of time that the allocations were exceeded, so that the science degradation could be incorporated into the data continuity budget. The analysis was conducted by embedding the spacecraft dynamic model inside a nonlinear simulation of the actuator electrodynamics, and driving the gimbals at representative speed profiles. The speed profile results were then combined to predict the net 24-hour jitter response for each of three phases of operation: +Z tracking, where the +Z antenna tracks the ground station and the -Z antenna is motionless; -Z tracking; and handoff, where the two antennae swap each half of the 24-hour orbit. The three operational phases are then combined to predict the distribution of HGAS-induced jitter over an entire year. This section will describe the models that are used to analyze HGAS jitter, the verification steps for the models, calibration activities, and validation of the model by test.

##### A. Model and Analysis Approach

The unpowered actuator dynamic stiffness is represented in the dynamic model using lumped masses and stiffnesses, and a Multi-Point Constraint (MPC) equation to represent the gearbox (Figure 8). The model includes the masses and inertias of the case, armature, and output shaft. The non-drive-axis stiffnesses (radial shear, bending, and axial stiffness) are represented with scalar springs. The unpowered holding torque (detent torque) of the actuator is represented with an equivalent torsional spring. The compliance

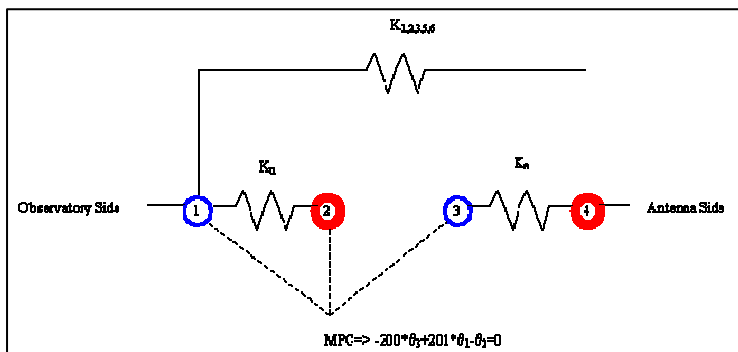


Figure 8 HGA actuator model in FEM

of the harmonic drive is reflected to the output of the gearbox and is represented as a torsional spring. The model is replicated four times, one for each of the actuators.

The actuator electrodynamic model is implemented as a Simulink(R) simulation. The electrodynamic torques include the powered and unpowered holding torques, and back-EMF torque. The simulation also includes Coulomb and viscous friction between the armature and case, and across the harmonic drive. The simulation torques are applied to the relevant nodes of the FEM. The nodal angles and rates are then fed back to the actuator model to compute the various angle- and rate-dependent torques. The simulation also includes a representation of the ACS and GCE processes that drive the antennas. This implementation enables accurate modeling of the various jitter mitigation approaches, namely stagger stepping and randomized stepping, for an arbitrary actuator profile<sup>8</sup>.

The actuator parameters include motor constant, motor inductance, detent torque, coulomb and viscous friction of various actuator components, etc. Where possible, parameters are directly measured and a parameter range is identified. Other parameters must be calibrated by tuning the model response to match measurement data. Calibration test results will be presented. An important point of note is that the initial parameters received from the actuator vendor were set by torque margin requirements, where higher friction is conservative. For jitter response, higher friction gives lower response. Therefore the lowest expected friction must be used for conservative jitter analysis. The baseline mechanical friction parameters used for jitter analysis were all extracted from calibration data.

Modal frequency uncertainty is handled somewhat differently for the HGAS Jitter analysis, as compared to other disturbance sources. The analysis assumes a constantly varying step rate, which will repeatedly cross critical structural frequencies. Therefore an error in prediction of modal frequencies will change the section of the actuator profile that results in peak jitter, but not in the peak jitter amplitude. Therefore the analysis is inherently insensitive to errors in modal frequency, and no additional steps are taken to account for it. Modal gain uncertainty is handled in the HGAS Jitter analysis identically to other sources, by holding out a margin requirement.

## **B. Model Verification**

The actuator model is verified by computing the bus and antenna rotation angles, after a single step is applied to one actuator. The true angles reached after such a move can be computed from the inertias of the bus and the antenna, and the offsets of each component's CG with respect to the hinge. The steady state angles from the simulation match the closed-form angles, confirming that the FEM modeshapes capture the inertia ratios and that the simulation conserves angular momentum. The simulation is also cross-checked against a Swales analysis code (TRONS) with good agreement.

## **C. Model Calibration**

The model is calibrated in three separate tests: winding voltage tests, which provide data on parameters that dominate the motion of the armature; actuator jitter tests, with the actuator driving a rigid load; and HGAS tap tests, to update the Finite Element model of the HGAS structure that filters the actuator torques before they reach the bus.

The winding voltage tests were conducted by stepping the actuator at various rates, and measuring the voltage across the redundant winding bleed resistor. Typical results are shown in Figure 9. The left plot shows the measured voltages for the three winding phases. The right plot shows the predicted voltages. The waveforms are captured very closely. There is a magnitude discrepancy of about 30%, possibly indicating some problem in the electrodynamic coupling model. However, the frequency and envelope are sufficient to validate the mechanical parameters for motor armature inertia and friction, and the powered and unpowered holding torques.

The second set of calibration tests to match harmonic drive parameters were conducted by mounting the actuator on a Kistler load table (Figure 10). Three different rigid load disks were fabricated, representing the range of inertias seen by the HGAS actuators, with inertias of 0.5 kg-m<sup>2</sup>, 1.0 kg-m<sup>2</sup>, and 2.0 kg-m<sup>2</sup>. The actuator was stepped at various rates and the reaction forces on the table were captured. The results were used to tune the harmonic drive stiffness and mechanical friction. The harmonic drive stiffness is nonlinear (it is a stiffening spring, with higher torque at larger angles), so the linear stiffness in the model was tuned for the particular amplitude of operation. The tests also showed that the mechanical friction is dominated by viscous (rate-dependent) friction, which increased at higher inertias (presumably because of axial loading of the shaft). The damping value from the lowest inertia was used as the baseline value, to give the most conservative jitter prediction. Figure 11 plots the measured and predicted reaction torques, after tuning, for a single step. The tuned model captures the frequency and ringdown decay very closely. The peak torque amplitude of the model is 4.3 N-m, very close to the measured 5.2 N-m peak.

The final set of calibration activities were performed on the HGAS structure itself, including everything outboard of the azimuth bracket. The HGAS was mounted to a Kistler table at the base of the azimuth bracket. Accelerometers were placed at the elevation actuator and at the back side of the boom, behind the dish. An instrumented hammer was used to tap the structure. FRFs between hammer inputs and Kistler and accelerometer

outputs were measured. System identification models of the FRFs were created and the modal frequencies below 200 Hz were used to tune the FEM. Initially the FEM showed the first few modes to be too soft, and the higher modes (above 80 Hz) to be too stiff. This is consistent with a mesh that is not fine enough. A detailed model of the azimuth bracket was developed and used to create a general stiffness element (GENEL) representation. Using this representation, the modal frequency error improved to 2% in the lower modes and 5% over all modes.

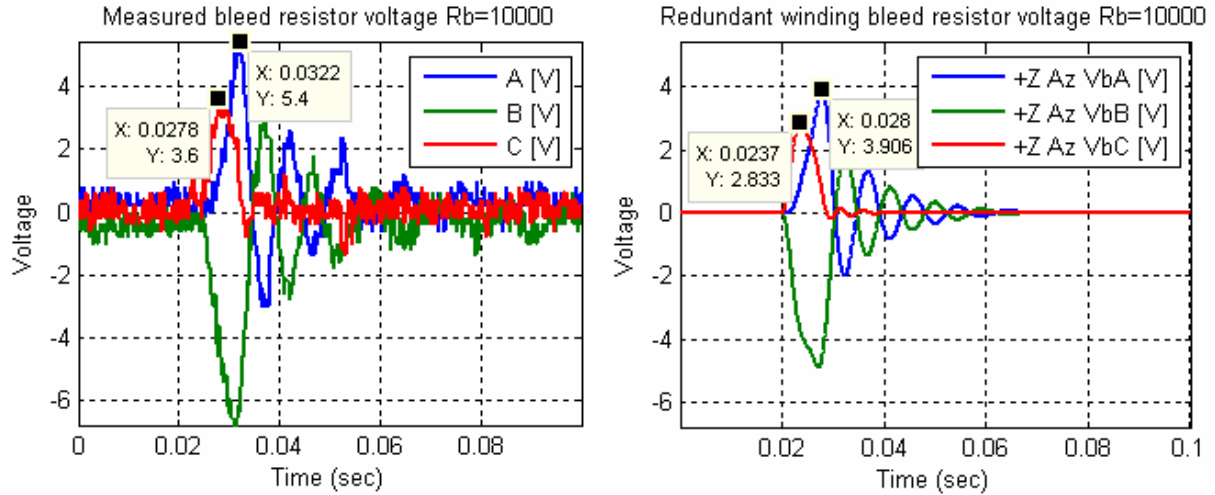


Figure 9 Winding voltage test results



Figure 10 Kistler table with HGA actuator and load disk

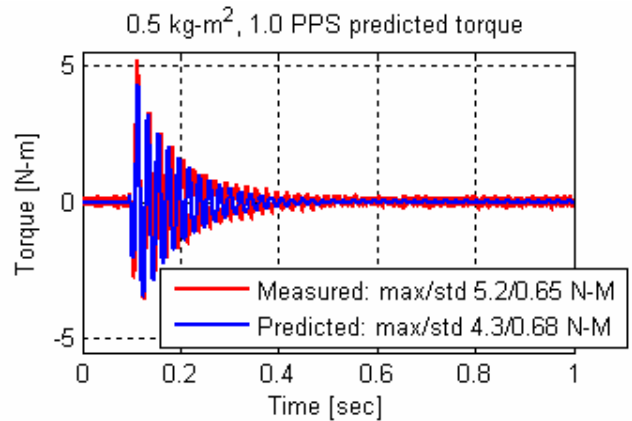


Figure 11 Reaction force from single HGA

#### D. Model Validation

The HGA Jitter model was validated by mounting the HGAS system to the Kistler table, and stepping through various move profiles. The Kistler table responses were acquired, processed to Power Spectra, and plotted against the predicted force/torque spectra. The tests were repeated at four different joint configurations, and at several step rates from 1 PPS to 66 PPS. Typical results for a 0.5 Hz step rate are shown in Figure 12. The plots show the six measured forces/torques, and the six predicted forces/torques. Note that a constant modal damping of 0.7%, equal to the average modal damping extracted from the tap test results, was used in the prediction. The predicted forcing is within a factor of two at all significant modes in the 10-100 Hz range.

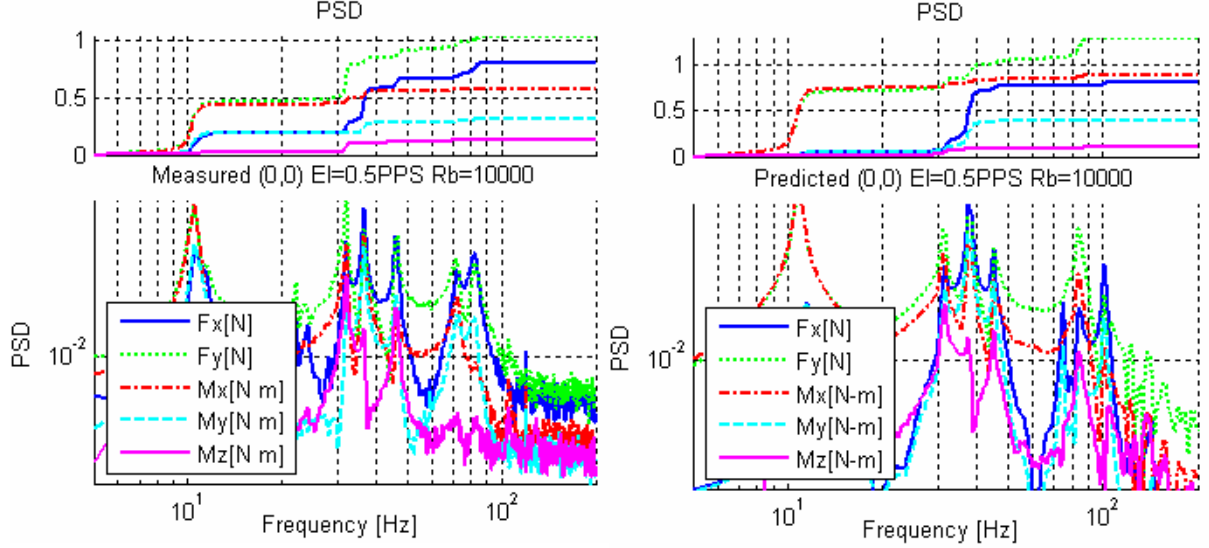


Figure 12 HGA validation results: (left) measured PSD (right) predicted PSD

## V. Reaction Wheel Disturbance Model

SDO has four Goodrich E-type reaction wheels onboard the spacecraft for attitude control. These wheels are mounted on the four upper bus panels of the spacecraft with the spin axis pointing 60 deg away from the body X axis. The maximum torque capability of each wheel is 0.25 Nm with a momentum limit of 70 Nms. The reaction wheels are well known sources of jitter disturbances<sup>5</sup> due to static imbalance, dynamic imbalance, and bearing imperfections that introduce tonal disturbances occurring at known ratios of the wheel speed. For SDO, the change in wheel speed is expected to be slow during science mode. As a result, the wheel tonal disturbances will have sufficient time to excite observatory structural modes and cause large vibrations. The techniques for analyzing tonal reaction wheel disturbances can be found in references 6 and 7. This section focuses on the wheel disturbance modeling approach, and verification, calibration, and validation of the wheel disturbance analysis.

### A. Modeling and Analysis Approach

The reaction wheel disturbance forces were measured by Goodrich in order to verify the imbalance requirements. The disturbance data were taken at a relatively coarse set of wheel speeds, in 60 revolutions per minute (RPM) steps. The tonal disturbances from the discrete data sets were unlikely to occur exactly at the frequency of a structural mode, and therefore the peak jitter would be missed. As an alternative, a semi-analytical wheel disturbance model was tuned to the test data. The model could then be stepped at a very fine wheel speed increment to ensure that the peak response was captured. The semi-analytical wheel model consisted of a physical model of the wheel axial and rocking modes, including gyroscopic torques on the wheel, excited by external forces. The Goodrich data exhibited two distinct forcing characteristics: tonal, wheel speed dependent disturbances at harmonics of the wheel speed, and broadband noise. Analysis demonstrated that both characteristics were important: the tonal disturbances were larger in magnitude and created the largest jitter response when the wheel harmonics crossed structural modes, but the broadband noise was always present and therefore continuously pumped energy into wheel structural modes.

The forcing characteristics were modeled by a speed-squared model for the harmonics, and a broadband noise spectrum for the remaining disturbance:

$$d(t) = \underbrace{\sum_{i=1}^{N_h} C_i f_{RW}^2 \sin(2\pi h_i f_{RW} t + \phi_i)}_{\text{Tonal/Harmonic Dist.}} + \underbrace{W(t)}_{\text{Random Dist.}} \quad (4)$$

where  $C_i$  is the amplitude coefficient,  $f_{RW}$  is the reaction wheel speed,  $h_i$  is the  $i^{\text{th}}$  harmonic number,  $\phi_i$  is the phase associated with the  $i^{\text{th}}$  harmonic, and  $W(t)$  is the random noise disturbance. The disturbance models were

created sequentially, with the harmonic model developed first (since the signal to noise is higher at the harmonics). The harmonics were then subtracted off to leave the broadband data. Attempts to fit a model to the broadband data gave unsatisfactory results, so the broadband data itself was used to perform the broadband analysis.

The harmonic disturbances were identified by using order analysis to transform the independent variable from frequency to harmonic factor (i.e., multiple of the wheel speed). Harmonic numbers  $h_i$  were then identified as ridges in the contour at constant harmonic factor. Each harmonic was then independently fit with a speed-squared model by simultaneously tuning the coefficient  $C_i$  and the structural model to the order analysis data (force/torque versus wheel speed) for that harmonic. Each of the four flight wheels was analyzed. Between 12 and 23 harmonics from 0.4 to 14.54 times the fundamental were identified. An example of the wheel radial disturbance torque ( $M_y$ ) is shown as a contour plot in Figure 13. The x and y axes of the plot are frequency and wheel speed, respectively. The dotted diagonal lines indicate the harmonic numbers identified for the wheel radial torque disturbance. The four wheels had many of the same lower harmonics (to about 9.0 times the fundamental), but the forcing levels at common harmonics can vary significantly between wheels, by up to a factor of 10.

The harmonic model was used to perform disturbance analysis by evaluating each harmonic at a vector of predefined wheel speeds, including the filtering from the wheel gyroelastic model. The vector was fine enough to give several points per half-power bandwidth of each of the spacecraft structural modes, so that the peak jitter was found. The random disturbance model was obtained directly from the power spectral densities (PSDs)  $S_{ww}(\omega)$  of the test data after extracting the harmonic disturbances. The random disturbance contribution to output performance can be computed easily using equation (1) stated in Section II, and the LOS PSD is calculated using the following equation<sup>6,7</sup>

$$S_{zz} = G_{zw} S_{ww} G_{zw}^H \quad (5)$$

where  $G_{zw}(\omega)$  is the transfer function from wheel disturbance  $w$  to LOS performance  $z$ . The responses due to each of the harmonics and the random disturbance were then root sum squared together, assuming the different disturbance components were uncorrelated. To understand the impact of modal frequency uncertainty, sensitivity analyses were done by shifting the disturbance frequency by small increments (1e-3 Hz). The largest LOS errors from the sensitivity analyses were reported as the CBEs.

## B. Model Verification and Calibration

For the reaction wheels, the disturbance model is based on the induced vibration data measured by Goodrich. Two analysts on the jitter team independently developed the wheel harmonic and random noise models and conducted wheel disturbance analyses to verify each other's results. The model parameters such as harmonic numbers and amplitudes, and reaction wheel structural modal frequencies were calibrated to the induced vibration data. As an example, Figure 14 shows the comparison between the radial moment data and the model fit for the fundamental harmonic ( $h_i=1.0$ ).

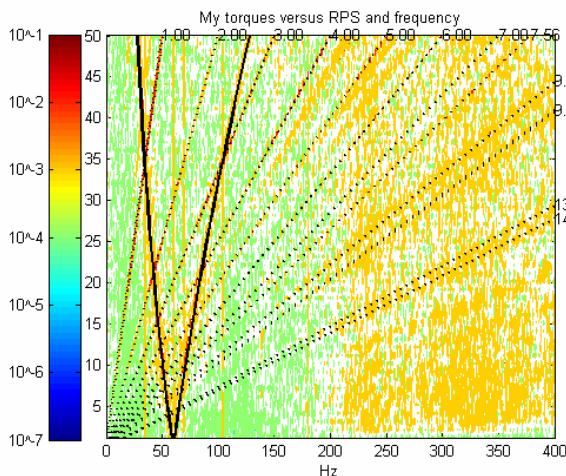


Figure 13 Contour plot of wheel torque

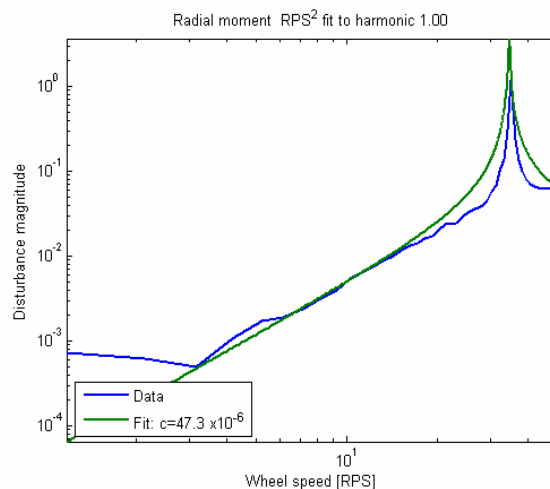


Figure 14 Radial moment fit to first harmonic

### C. Model Validation

In order to validate the reaction wheel disturbance model and analysis approach, one of the flight wheels was mounted on the Structural Verification Unit with complete wheel electronic integration. A sketch of the setup is shown in Figure 15. The software for the wheel test incorporated a simple proportional-integrator controller developed to control the wheel speed using the wheel tachometer feedback. The control software was loaded to the SDO Attitude Control Electronics (ACE) engineering test unit (ETU). The ETU ACE/wheel telemetry, including torque commands, motor current, and tachometer pulse counts, was monitored by the NTGSE and the ASIST workstation. The NTGSE is a Bus Controller Simulator (BCS) that provides the 1553 interface to the ACE. The ASIST workstation is a PC which, when used in conjunction with the BCS, simulates the Single Board Computer (SBC) and the ground station. This computer tool allowed the testers to interact with the flight software loaded in the ACE.

As the flight wheel excited the SVU structure, tri-axial accelerometers mounted at each of the four AIA telescopes, the HMI instrument, and the three bus-instrument module interface locations measured the jitter vibration levels. All the test data were logged using the DataPhysics system at a sample rate of 1024 Hz. An additional tri-axial accelerometer was mounted at the flight wheel housing. This measurement showed a strong response component at the wheel spin rate, and provided a more accurate measure of the wheel speed than the tachometer.

During the flight wheel tests two operating modes were employed. First, the flight software commanded the ACE to drive the wheel to a specific wheel speed and hold the speed constant for the duration of the dwell speed tests (2-5 min.). Second, the flight software commanded the wheel to ramp the speed at a fixed rate of acceleration (0.1 RPM/sec or 1.0 RPM/sec). The ramp speed tests helped the test engineers to identify problematic wheel speed ranges that correspond to large jitter motions observed at the instruments. The test engineers then targeted those speed ranges using the dwell speed mode.

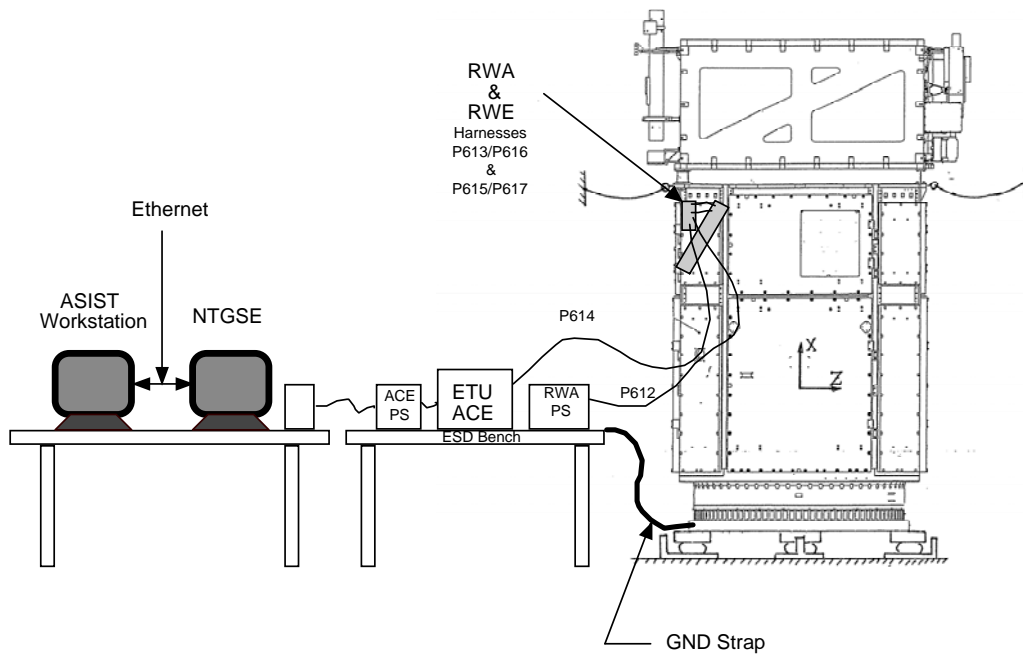


**Figure 15 SVU and flight wheel jitter test setup**

A representative set of the wheel ramp results are shown in Figure 16. The blue crosses represent the root-mean-square (RMS) acceleration data measured during the tests, the dashed line shows the analytical prediction using the disturbance model and analysis described above plus the background noise, and the solid constant line indicates the background noise level during the tests. The plots in the top row illustrate RMS accelerations at AIA telescope #3 during the low acceleration (0.1 RPM/sec), ramp speed test. This test focuses on measuring disturbances at low wheel speeds (<700 RPM) which correspond to the expected wheel speed operational range on orbit. From Figure 16 and other test data, the results show that our analytical prediction is generally a factor of 1.5 to 2.0 larger than the

measured accelerations. Based on this observation, the required jitter analysis margin on the wheel disturbances was reduced from 100% to 66.7%. The plots on the bottom row of Figure 16 show the acceleration measurements from the same location during the high acceleration (1.0 RPM/sec) ramp speed test. At high wheel speeds (>700 RPM), the analysis prediction follows the measured data surprisingly well given the uncertainties in the structural FEM. The flight wheel plus SVU jitter tests validated the modeling and analysis approach used for SDO.

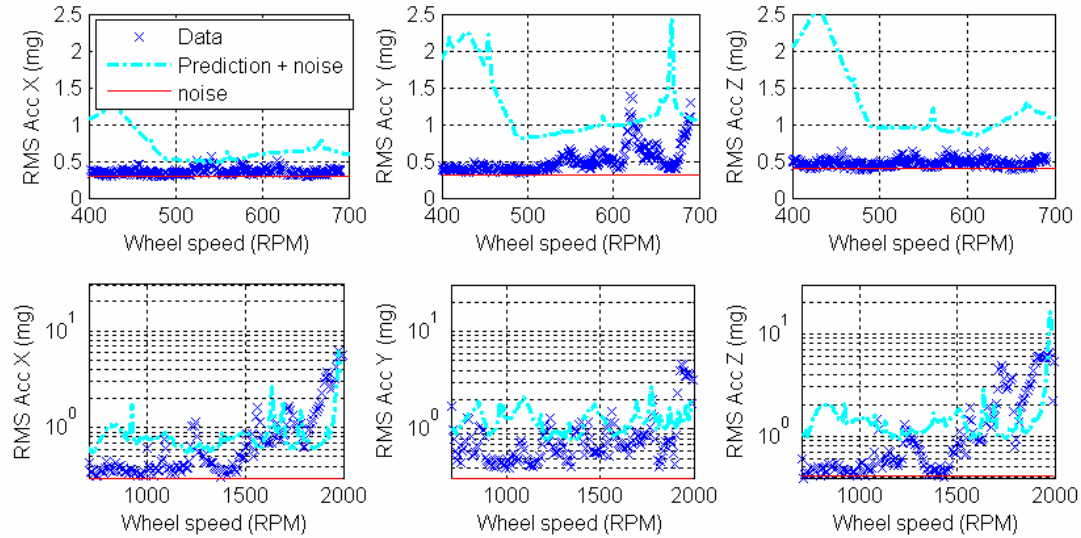


**Figure 16 SVU wheel jitter results: (top) low wheel speed (bottom) high wheel speed**

## VI. On-orbit Mitigation Strategies and Test Plans

Although detailed analysis and assembly level tests were performed in order to obtain good jitter predictions, there are still several sources of uncertainties in the system. The structural finite element model will not have all the modes correlated to test data at high frequencies (>50 Hz). The performance of the instrument stabilization system will not be known exactly but should be close to the analytical model. A true disturbance-to-LOS observatory level test will not be available due to the tight schedule of the flight spacecraft, the cost in time and manpower, difficulties in creating gravity negation systems, and risks of damaging flight hardware. To protect the observatory jitter performance against model uncertainties, the jitter team has devised several on-orbit contingency plans in addition to reserve margins on analysis results.

Extensive HGA pointing algorithm modifications were recommended to mitigate HGA jitter issues. Due to the large scope of this work, a separate paper is written (Ref. 8) to describe the details of the HGA pointing algorithm and jitter mitigation strategies. In this section, the on-orbit instrument and reaction wheel mitigation strategies test plans are presented.

### A. EVE Instrument

Although the EVE instrument does not have tight jitter requirements, it contains four noisy filter wheels driven by stepper motors. The EVE filter wheel is another large disturbance contributor after the HGAs and the reaction wheels, but it does not operate as frequently as the other two jitter sources. Each of the four EVE filter wheels is expected to move 10 min per day with a total of 40 min operational time per day. Since the step rates of the EVE filter wheels are tunable, the team plans to vary the step rates after SDO gets in orbit and determine which step rate should be used to minimize jitter.

For the on-orbit jitter tests, the instrument limb sensors can be used to measure jitter vibrations. These sensors are also used as feedback signals for the AIA and HMI ISS with an update rate of 256 Hz. During the jitter tests, the ISS loop can be opened to allow larger jitter signals to be measured. Each of the four EVE filter wheels will be commanded to spin at a pre-specified rate for about a minute while the AIA and HMI limb sensors record the jitter data. The RMS of the jitter time-history data will be computed and used to determine which step rate should be used during nominal EVE operations.

## B. Reaction Wheel

Since SDO is sun-pointing, and since it is fairly symmetric about the sun line, the solar torques acting on SDO are relatively low. As a result, the ACS team has considerable freedom to reduce the reaction wheel speed range in order to reduce reaction wheel disturbances. In general larger wheel disturbances are generated at higher wheel speeds. Based on wheel jitter predictions, the wheel speeds are nominally limited to 400 RPM (out of the ~3000 RPM momentum limit) in order to satisfy the wheel jitter requirement. Once SDO gets on orbit, the team plans to test the wheel-induced jitter, and will try to extend the wheel speed limit if possible.

The on-orbit tests for the reaction wheels are intended to identify the impact of the wheel-induced disturbances on spacecraft jitter at wheel speeds outside the prescribed nominal operating range. The basic principle behind the tests is to slew one wheel at a time in the speed range of interest while ensuring that the remaining wheels stay inside the prescribed nominal range. Thus a large jitter response can be associated with the slewing wheel. The speed slew range is limited to 800 RPM since the other wheels must remain in the nominal range. The attitude control system's Delta-H and Science modes are used to bias the targeted wheel to a prescribed speed outside the nominal range, while the remaining three wheels are biased at either extremes of the nominal range (+400 or -400 RPM). The spacecraft jitter is sensed via the two limb sensors within the AIA and the HMI instruments. The tests will enable the measurement of the true jitter-limited wheel speed range. The algorithm for the on-orbit wheel jitter tests is summarized in the following:

- a) Implement a digital low pass filter to attenuate the high frequency noise in the measured wheel momentum signals from tachometers.
- b) Compute the initial desired momentum bias in the body frame, and invoke the Delta-H and Science modes to take the wheel speeds from their current values to their desired values. It is assumed that the wheel speeds have reached steady-state prior to start of the wheel jitter test. SDO employs four reaction wheels in a pyramid configuration about the body X axis, i.e., there are two pairs of opposing wheels tilted away from the X axis towards Y and Z axes, respectively. For example, if we assume that the targeted wheel is wheel no. 1, and it is desired to slew that wheel from an initial wheel speed of  $w_0$  to  $w_0 + 800$ , then the initial wheel speeds for the other three wheels must be set to [400 -400 400] RPM, respectively. The negative speed corresponds to wheel no.3 which is the wheel that opposes wheel no. 1.
- d) Set the initial value of the slew torque commands to the bias values

$$T_{slew} = T_{bias} * N_w$$

Where  $T_{bias}$  represents the torque bias, and  $N_w$  denotes the null vector in the wheel space.  $T_{bias}$  is chosen to provide a desired slew rate for the targeted wheel.

- e) At every minor cycle (40 seconds), compute the difference in the current wheel momentum and the momentum in the previous cycle for the target wheel.

$$wd = wh_k(i) - wh_{k-1}(i)$$

Where index "i" denotes the target wheel, the index "k" refers to the current cycle, and the index "k-1" refers to the previous cycle.

- f) If  $|wd| \leq wd_{lim}$ , apply a delta correction to the slew torque commands to increase the slew rate:

$$T_{slew} = T_{slew} + T_{corr} * N_v$$

Where  $T_{corr}$  represents the scale of the torque correction, and is computed as follows.

$$T_{corr} = \alpha * \text{sgn}(T_{bias}) * \left( |wd| - wd_{lim} \right)$$

Where  $\alpha$  is scale factor chosen at 0.025.

- g) Stop the experiment when either the target wheel speed reaches its final prescribed wheel speed, or the absolute value of the speed of one or more of the supporting wheels reaches the maximum allowed range.

The wheel slew algorithm was implemented within the high-fidelity simulation. This simulation includes detailed models of components and ACS modes, as well as structural dynamics. The flexible dynamics are represented by the finite element model normal modes. Figure 17 and Figure 18 illustrate a simulation run with wheel no. 1 as the targeted wheel. The wheel was slewed from 2200 RPM to just over 2500 RPM in about 1500 seconds. Here, the initial speeds for wheels no. 2-4 were chosen as [350 -350 350] RPM, respectively. Note that these wheels remain in the allowable range during the course of the test. Figure 18 illustrates the LOS jitter at the CCD of the HMI instrument. Significant excursions, exceeding the HMI wheel allocation of 60 mas, are observed at wheel speeds of 2300-2400 RPM.

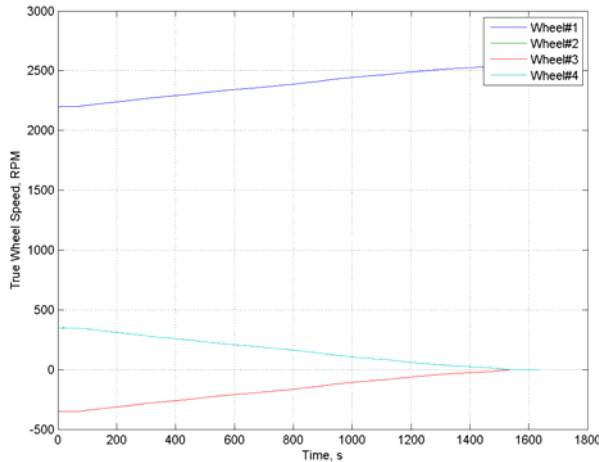


Figure 17 True Wheel Speeds

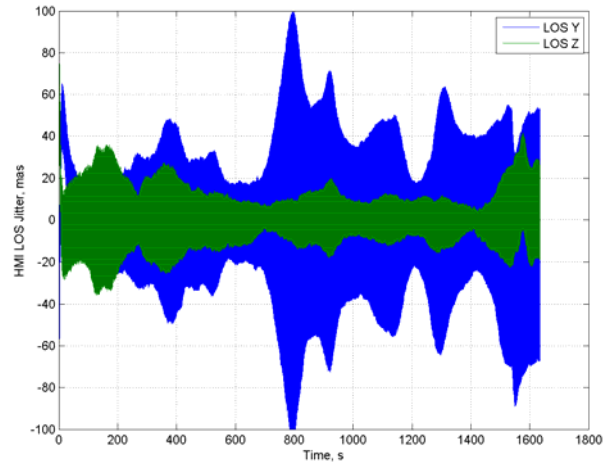


Figure 18 HMI Line-of-Sight Jitter

## VII. Summary and Lessons Learned

This paper describes the tests used to support SDO jitter analysis and on-orbit jitter mitigation. It begins with an overview of the SDO jitter analysis approach. Methodologies, tests, and test results for verifying, calibrating, and validating models of the major jitter sources are presented. In recognition of the fact that model uncertainties still exist even after extensive model correlation effort, the paper then lays out the mitigation strategies and on-orbit jitter test plans that were developed to accommodate unpredicted on-orbit jitter problems. Jitter predictions based on the calibrated models indicate that SDO will have an acceptable level of jitter. In conjunction with the on-orbit jitter mitigation, there is high confidence that SDO will meet its stringent jitter requirements. After spending almost three years of analysis and test effort on the SDO jitter problem, the SDO jitter team has the following lessons learned to share with the community:

- For jitter sensitive missions (sub-arcsecond level requirements):
  - Perform early jitter assessments to identify what protective steps are necessary.
  - Instrument mechanisms: vary step frequency or commutation frequency on-orbit to avoid exciting structural modes
  - Reaction wheels: develop specs for higher harmonics and random noise components
  - HGA: consider micro-stepping and implement pointing algorithm to allow random and stagger stepping
  - Provide for coordination between telescope and mechanism operations
  - Provide for on-orbit jitter assessment, to support modification of mechanism operational modes
- Every disturbance source should be measured as early as possible
  - Simple mechanism models may not account for gears, backlash, higher harmonics, etc
  - A test facility should be set up to test all mechanisms
  - Measurement system must be well calibrated before tests
- Plan model verification, validation, and calibration work early
  - Calibrate component models and validate at systems level (as close to flight configuration as possible)

- Accuracy of system model is bounded by accuracy of component models (usually worse due to uncertainty at mounting interfaces)
- Damping ratio of 0.3% is a good number for jitter analysis for conventional structural system at typical temperature range (non-cryogenic)
  - Suggested damping value is a good starting point but should be verified by test
- An isolation system *might* be beneficial
  - At reaction wheel mounting interface, if speed cannot be limited
  - At instrument interface
  - Waiting until jitter analysis is complete before deciding on the implementation of an isolation system will likely be too late

## VIII. References

- 1 Mark E. Pittelkau, “Definitions, Metrics, and Algorithms for Displacement, Jitter, and Stability,” *AAS Guidance and Control Conference*, 03-559, 2003.
- 2 “ASME Guide for Verification and Validation in Computational Solid Mechanics”, March 29, 2006.
- 3 “Guide for the Verification and Validation of Computational Fluid Dynamics Simulations”, *American Institute of Aeronautics and Astronautics*, 1998, Reston, Va.
- 4 S. Starin, K. Bourkland, K. Liu, P. Mason, M. Vess, S. Andrews, and W. Morgenstern, “Attitude Control System Design for the Solar Dynamics Observatory,” *Flight Mechanics Symposium*, NASA Goddard Space Flight Center, October 2005.
- 5 Bill Bialke, “A Compilation of Reaction Wheel Induced Spacecraft Disturbances,” *AAS Guidance and Control Conference*, 1997.
- 6 Homero Gutierrez, “Performance Assessment and Enhancement of Precision Controlled Structures During Conceptual Design,” PhD thesis, MIT Department of Aeronautics and Astronautics, 1999.
- 7 K. Liu, P. Mulé, T. Kenney, and C. Blaurock, “Dynamic Jitter Modeling and Analysis of Solar Dynamic Observatory,” *Flight Mechanics Symposium*, NASA Goddard Space Flight Center, October 2005.
- 8 K. Bourkland, K. Liu, and C. Blaurock, A Jitter-Mitigating High Gain Antenna Pointing Algorithm for the Solar Dynamics Observatory,” *20<sup>th</sup> International Symposium on Space Flight Mechanics*, NASA Goddard Space Flight Center, September 2007.